

Short Communication

## Facile Synthesis of Hexagonal CdS Nanofilm on FTO Glass Substrate via Hydrothermal Method

Yang Tan<sup>&,1</sup>, Zheng Zhang<sup>&,1</sup>, Fuqiang Guo<sup>1,\*</sup>, Renqing Guo<sup>2,\*</sup>, Haineng Bai<sup>3,\*</sup>, Baohua Zhang<sup>1</sup>, Xin Li<sup>1</sup>, QianYang<sup>1</sup>, Xuebo Liu<sup>1</sup>

<sup>1</sup> Department of Physics, Changji University, Changji 831100, China

<sup>2</sup> Department of Materials Engineering, Taizhou University, Taizhou 318000, China

<sup>3</sup> National Laboratory of Solid State Microstructures, Nanjing University, Nanjing 210093, China

& These authors contributed equally to this work

\*E-mail: [cjxyedu@163.com](mailto:cjxyedu@163.com), [guorqing@126.com](mailto:guorqing@126.com), [bhn9052nju@163.com](mailto:bhn9052nju@163.com)

Received: 5 July 2020 / Accepted: 19 August 2020 / Published: 31 August 2020

---

In this work, the compact CdS nanofilm has been deposited on FTO glass substrate with the conductive side facing down by the hydrothermal method. The microstructure and morphology of nanofilm were respectively analyzed by X-ray diffraction (XRD), scanning electron microscopy (SEM) and transmission electron microscopy (TEM). The results exhibited hexagonal wurtzite CdS nanofilm and continuously dense. Besides, the growth mechanism of CdS nanofilm was discussed and explored in detail: the small amount of CdS nuclei can crystallize during the initial reaction and form a CdS thin layer on the conductive side of FTO glass substrate; thereafter, with increasing temperature, many CdS nuclei can crystallize and grow on the CdS thin layer. Also, the photoelectric properties of nanofilm were studied by photoluminescence spectrum (PL), Raman spectrum, transient photocurrent response and electrochemical impedance spectroscopy (EIS).

---

**Keywords:** CdS nanofilm; hydrothermal method; CdS thin layer; FTO glass substrate; growth mechanism;

### 1. INTRODUCTION

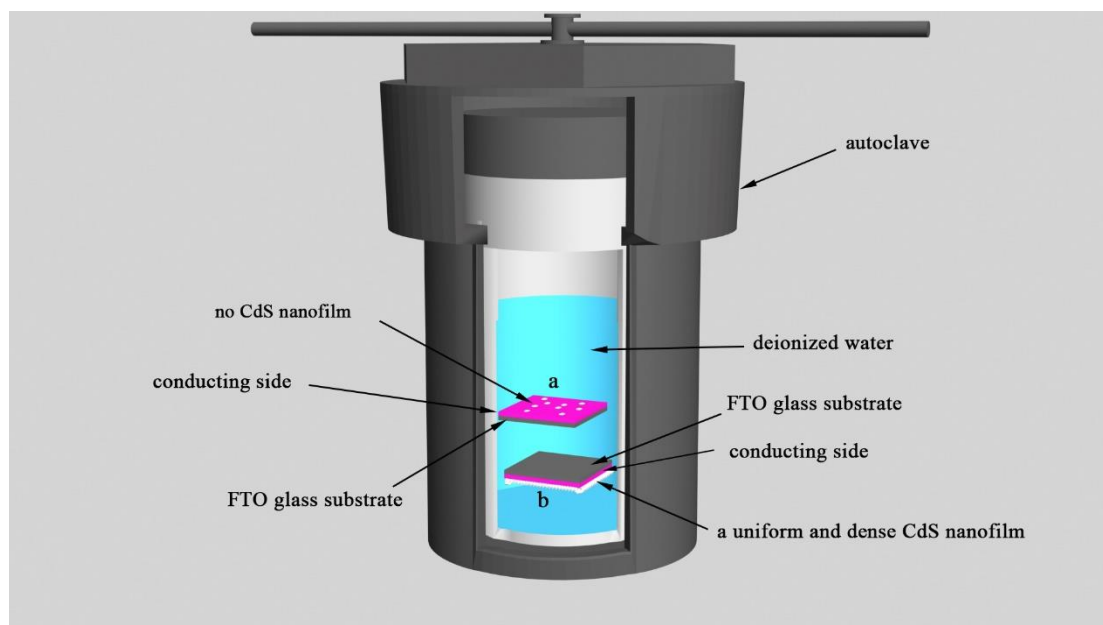
Cadmium sulfide (CdS,  $E_g=2.42\text{eV}$ ) was considered a significant II-VI group semiconductor material [1]. It had excellent photoelectric conversion characteristics and light absorption properties. Therefore, CdS can be utilized in solar cell [2], photosensor [3], photodiode [4]. In recent years, different sizes and morphologies of the CdS have been successfully prepared to study the properties [5], such as quantum dots [6], nanorods [7,8], nanoflowers [9] and nanoarrays [10]. Numbers of synthesised CdS nanofilm methods have also been used, including chemical bath deposition [11], electron beam evaporation [12], Sol-gel method [13], and magnetron sputtering method [14]. He et al.

[15] have prepared CdS thin film by chemical bath deposition, and explained the growth mechanism of thin film. Abdel Galil et al. [16] have deposited CdS thin film by electron beam evaporation, and prepared CdS powder by hydrothermal method to explore solar cell devices. Nevertheless, the above methods have some drawbacks, such as high energy requirements, high vacuum, and expensive equipment. Therefore, seeking an effective and inexpensive method is crucial to controlling the morphology of CdS nanofilm. Notably, the hydrothermal method has been regarded as the most promising method with the advantages of single-step process, high product purity and homogeneity [17]. In our previous work, ethylenediamine and deionized water were applied to facilitate the thin film's growth. A uniform and dense nanorod-shaped CdS nanofilm [18] and hexagonal CdS nanofilm [19] were successfully synthesized on Al<sub>2</sub>O<sub>3</sub> substrate. However, CdS nanofilm has less optical properties. Following, the hexagonal CdS nanofilm was successfully synthesized on the smooth FTO glass substrate by the hydrothermal method. It was beneficial to form a uniform and dense nanofilm with the conductive side of the FTO glass substrate facing down. However, when the conductive side was facing up, the CdS nanofilm was not easy to form. In this work, the growth mechanism, microstructure, morphology and photoelectric properties of CdS nanofilm grown on FTO glass substrate with the conductive surface facing down were explored.

## 2. EXPERIMENTAL SECTION

All reagents were of analytical grade and can be used without further purification. In a typical procedure, cadmium chloride (CdCl<sub>2</sub>·2.5H<sub>2</sub>O), thiourea ((NH<sub>2</sub>)<sub>2</sub>CS, Tu), L-cysteine, acetone and ethanol absolute were purchased from Sinopharm Chemical Reagent Co., Ltd., respectively. FTO glass substrate and deionized water were gained from local sources.

The hydrothermal method was used to prepare CdS nanofilm with the conductive side facing up and down, as shown in Scheme 1. In a typical synthesis, initially, 40 mL of deionized water was added to a Teflon-lined stainless steel autoclave (50mL capacity). Then, 5 mmol CdCl<sub>2</sub>·2.5H<sub>2</sub>O, 8 mmol Tu, and 2 mmol L-cysteine were dissolved to the autoclave, respectively, stirred for 10 minutes with magnetic stirrer. In the meantime, two slices of the FTO glass substrates have been ultrasonically cleaned for 15 min in acetone, ethanol absolute and deionized water, respectively. Thereafter, two slices of the FTO glass substrate were flatly placed in the bottom of the autoclave with conductive faces up and down, respectively. The hydrothermal reaction was performed at 160°C for 10 h. When the autoclave was naturally cooled to room temperature, the obtained samples were repeatedly filtered and washed several times with deionized water and ethanol absolute, and then dried at 60°C for 12 h.



**Scheme 1.** Preparation of CdS nanofilm grown on FTO glass substrates with the conducting side facing (a) up and (b) down, respectively

The crystal structure of the sample was confirmed by XRD on a Japanese Mac Science 18Kw rotor diffractometer with graphite monochromated Cu K $\alpha$  radiation ( $\lambda = 0.1540560$  nm), employing a scanning rate of  $0.1^{\circ}\text{s}^{-1}$  and  $2\theta$  ranging from  $20^{\circ}$  to  $70^{\circ}$ . The surface morphology of the sample was characterized by SEM (Hitachi, S-4800) equipped with an energy dispersive X-ray spectrometer (EDS). The morphology and microstructure of the sample were analyzed by TEM (JEM-200CX) and high-resolution transmission electron microscope (HRTEM) (JEOL-2010). A fluorescence spectrophotometer measured PL spectrum at room temperature (ZLX-PL-I,  $\lambda=325$  nm). The Raman spectrum was tested by Laser confocal Raman spectrometer at room temperature (JYHR800,  $\lambda= 514$  nm). The transient photocurrent response and EIS of CdS nanofilm with the conductive side of the FTO glass substrate facing down was measured on an Electrochemical Workstation (CHI-760E, China). The transient photocurrent response of the prepared CdS nanofilm with an area of  $1\text{ cm}^2$  was evaluated under a visible light irradiation (light on–off cycles: 20 s) at a fixed electrode potential of 1.23 V versus reversible hydrogen electrode (RHE).

### 3. RESULTS AND DISCUSSION

#### 3.1. SEM analysis

Morphologies of CdS nanofilm grown on FTO glass substrates with conductive side facing up and down were respectively depicted in Fig. 1 (a) and (b) (c). Fig. 1 (a) showed small, irregular nanoparticles, implying the thin film was not easy to grow. However, Fig. 1 (b) can be observed that the CdS nanofilm was a hexagonal shape, smooth, uniform and dense. It meant that the sample had a better crystallinity. Fig. 1 (c) depicted that the side length, thickness, and diameter of CdS nanofilm

was about 140nm, 90nm, and 280nm.

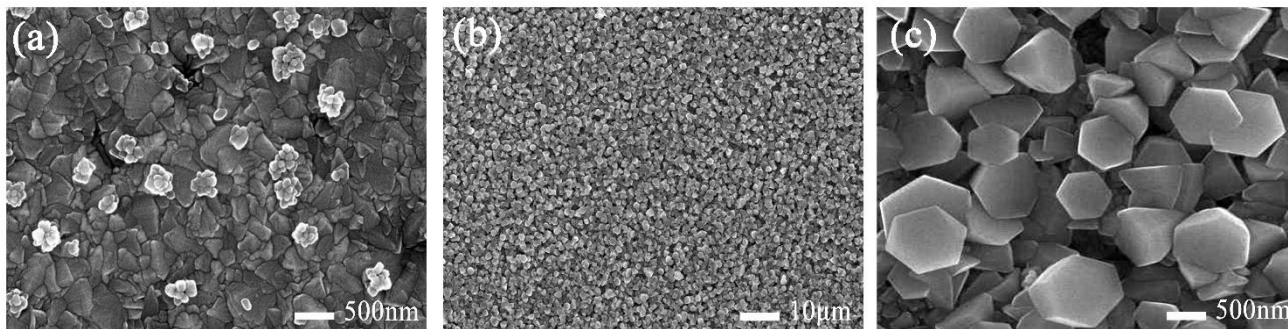


**Figure 1.** SEM images of CdS nanofilm grown on FTO glass substrates with conducting side facing (a) up and (b, c) down, respectively

### 3.2. XRD analysis

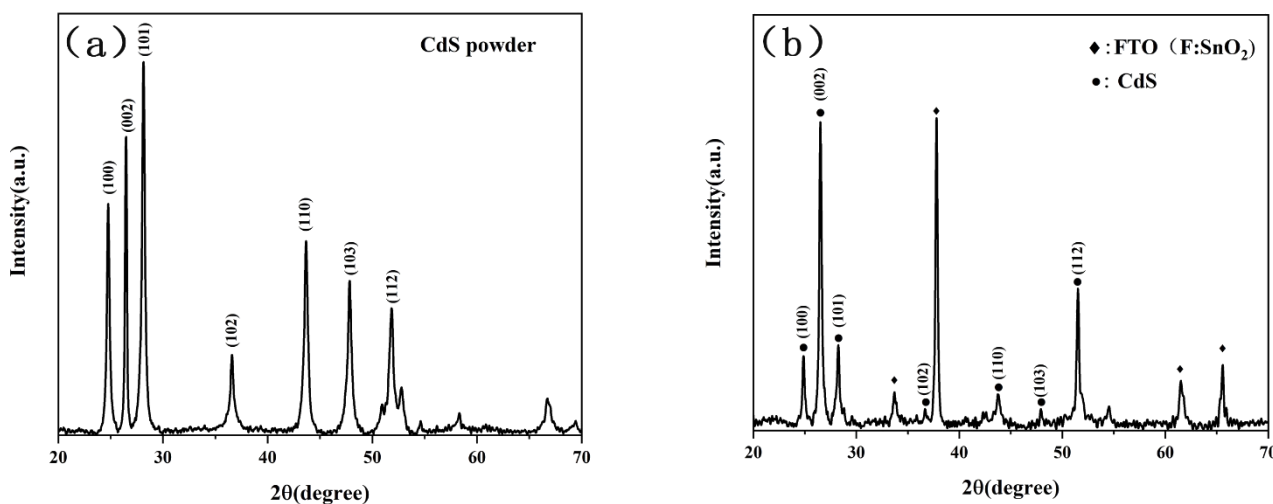


**Figure 2.** XRD patterns of (a) CdS powder and (b) CdS nanofilm grown on FTO glass substrate with conductive side facing down

The XRD patterns of CdS powder (a) and CdS nanofilm grown on FTO glass substrate with the conductive side facing down (b) were displayed in Fig. 2. It can be revealed that the main diffraction peaks located at  $2\theta \approx 24.78^\circ$ ,  $26.48^\circ$ ,  $28.16^\circ$ ,  $36.61^\circ$ ,  $43.71^\circ$ ,  $47.85^\circ$ , and  $51.86^\circ$ , corresponding to the (100), (002), (101), (102), (110), (103) and (112) planes of hexagonal wurtzite CdS (ICDD PDF No. 41-1049) and the calculated values of the lattice constants were  $a \approx b \approx 4.143\text{\AA}$  and  $c \approx 6.724\text{\AA}$ . Furthermore, the main diffraction peaks had high intensity and sharpness in Fig. 2 (a) and (b), indicating that the samples had better crystallinity. The diffraction peaks marked with an asterisk in Fig. 2 (b) were associated with FTO glass substrates containing SnO<sub>2</sub> of F. Fig. 2 (b) can be found that the

intensity of the diffraction peak corresponding to (002) plane was stronger than (101) and (100) planes, implying that the sample had a preferential growth trend.

### 3.3. TEM and EDS analysis

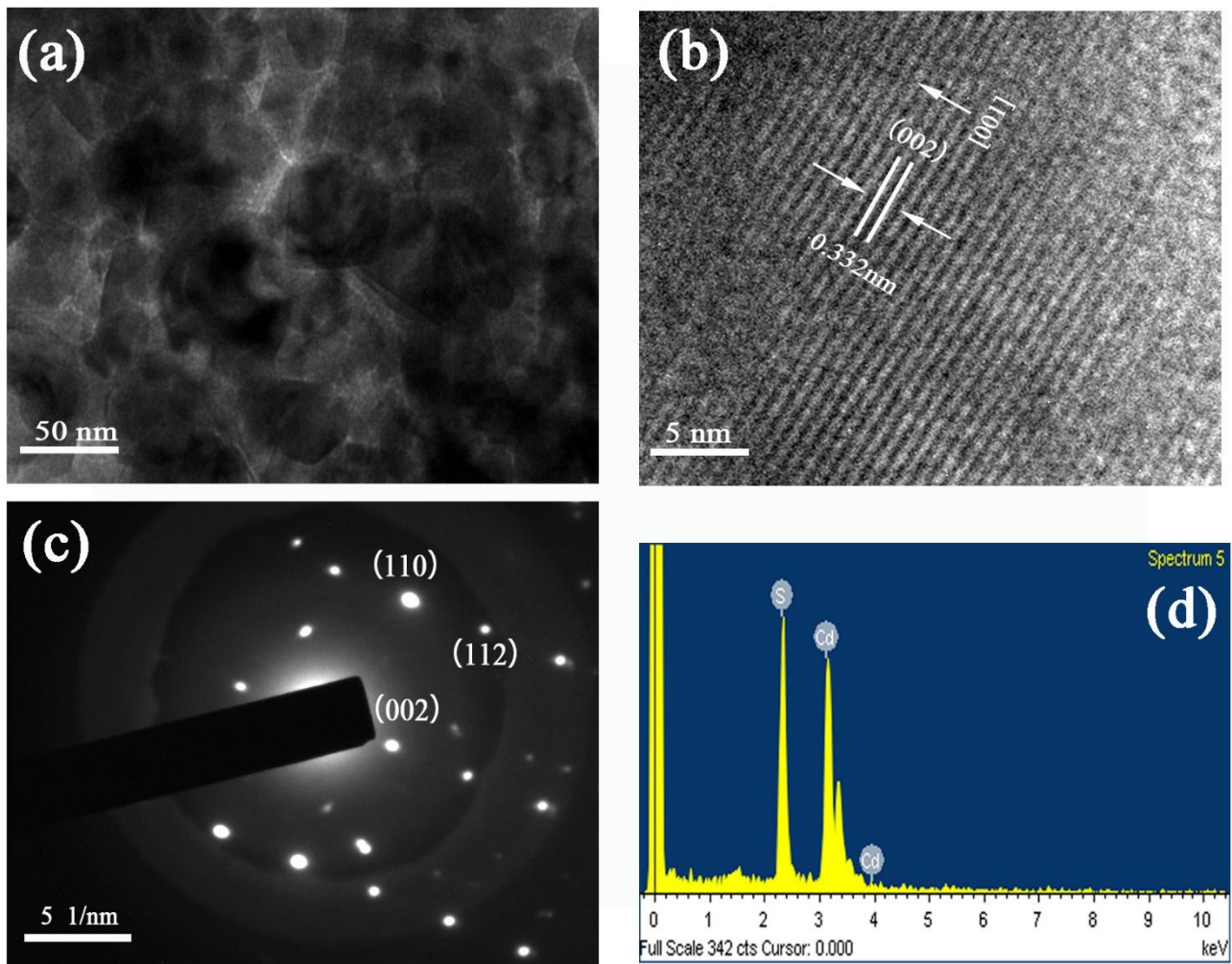


**Figure 3.** (a) TEM, (b) HRTEM, (c) selected area electron diffraction (SAED) and (d) EDS images of CdS nanofilm grown on the FTO substrate with conducting side facing down

The morphology, microstructure, and elemental analysis of CdS nanofilm grown on the FTO glass substrate with the conductive side facing down were further analyzed by TEM, HRTEM, SAED, and EDS, as shown in Fig. 3. Fig. 3 (a) displayed hexagonal morphology, and the thin film connection was relatively tight; the diameter of hexagonal CdS nanofilm was about 298nm. Fig. 3 (b) exhibited that the lattice distance of 0.332 nm matched the interplane distance of (002) crystal plane, implying that the [001] direction was perpendicular to the basal plane of the crystals. The SAED pattern showed that the CdS nanofilm had a hexagonal wurtzite structure in Fig. 3 (c) [19]. The EDS pattern (Fig. 3 (d))

displayed that CdS nanofilm was composed of 45.25% Cd element and 52.89% S element and the atomic ratio closed to 1: 1, indicating that the sample had a pure phase.

### 3.4. PL studies

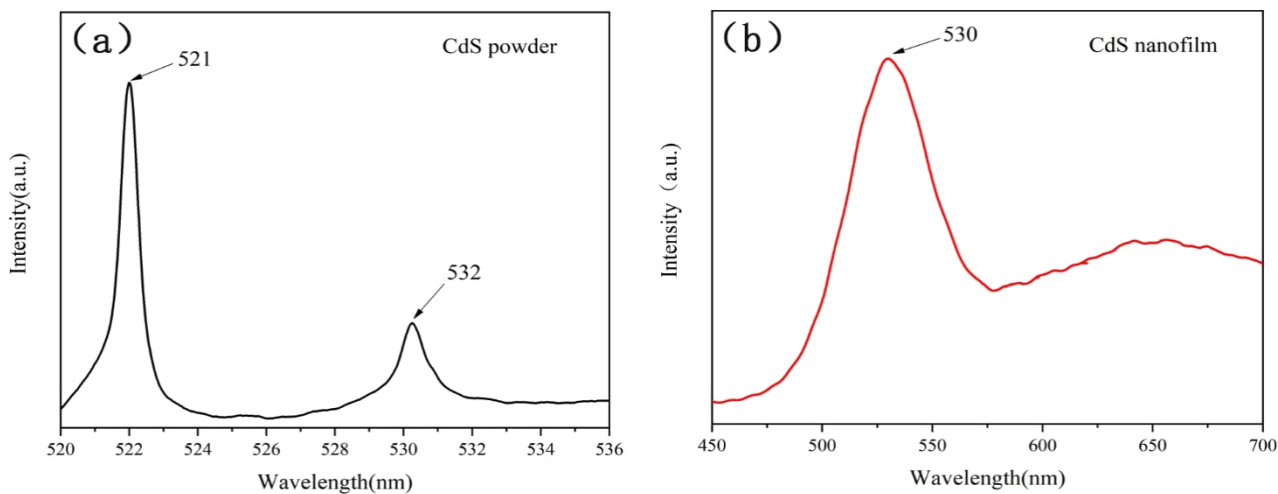


**Figure 4.** PL spectrums of (a) CdS powder and (b) CdS nanofilm grown on FTO glass substrate with conducting side facing down

The size and morphology of the sample had an essential effect on PL properties. Therefore, Fig. 4 displayed the PL spectrum of CdS powder and nanofilm using excitation wavelength of 325 nm at room temperature. The characteristics of the PL spectrum were explored. Fig. 4 (a) displayed that CdS powder had two excitation peaks, one of which was stronger at 521nm and the other weaker at 532 nm. The peak of the former was sharper than the peak of the latter. However, Fig. 4 (b) depicted significant excitation peak of the CdS nanofilm was located at 530 nm. Two excitation peaks of CdS powder correspond to the CdS band gap width of 2.38 eV and 2.33 eV, respectively, and CdS nanofilm correspond to a CdS band gap width of 2.34 eV [20]. It demonstrated a slight redshift compared with the wavelength position of CdS material (512 nm) [18]. The interface effect and the crystal structure might be caused by the slight redshift of the sample. At the same time, there were maybe two additional reasons for the small redshift of the CdS sample. Firstly,  $\text{Cd}^{2+}$  and  $\text{S}^{2-}$  ion vacancies might exist on the nanofilm surface, promoting the redshift of the thin film [21]. Secondly, CdS powder had not yet been converted, and it might also cause a redshift [22].

### 3.5. Raman spectrum analysis

The Raman spectrum was performed with an excitation wavelength of 514 nm to explore the structure and performances of the sample in Fig. 5. It can be observed that the peaks of the CdS powder and CdS nanofilm were located at  $299\text{ cm}^{-1}$  and  $300\text{ cm}^{-1}$ , respectively, which can be regarded

as the  $A_1$  (1LO) mode (where LO was the longitudinal optical phonon). Further, full width at half maxima (FWHM) was  $12.95\text{ cm}^{-1}$ , and  $14.1\text{ cm}^{-1}$  and overtones were  $598\text{ cm}^{-1}$  and  $600\text{ cm}^{-1}$ , respectively, which can be regarded as  $A_1$  (2LO) mode of CdS material [23]. Compared with the 1LO peak position of the CdS material ( $305\text{ cm}^{-1}$ ), the Raman spectrum of the as-prepared CdS material had a moderate redshift [20]. The mini size effect of the sample might be responsible for the redshift of the peak position. Besides, the thin film's peak intensity was slightly stronger than the powder, and it might be due to the lattice distortion in the CdS nanoparticle. However, in Fig. 5, sharp peaks of the 1LO and 2LO were observed between  $250\sim 700\text{ cm}^{-1}$ . There were no additional vibration mode peaks, and it was consistent with related literature reports [24].

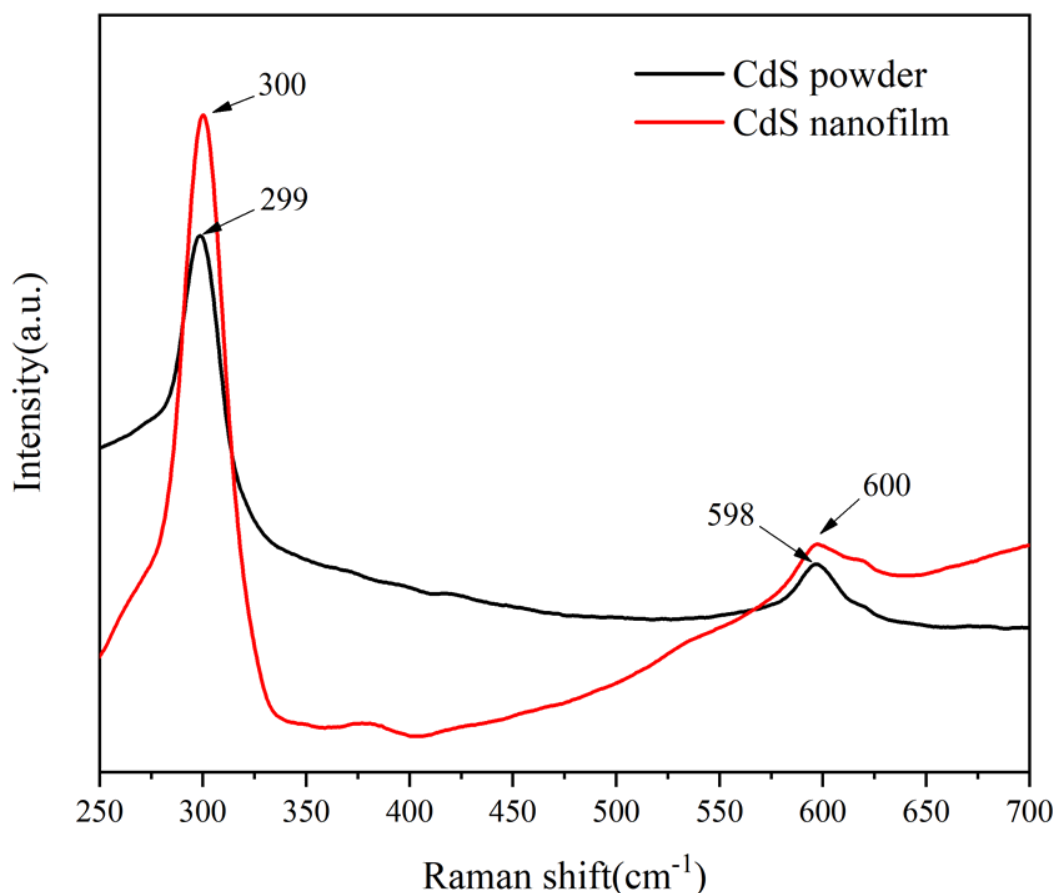


**Figure 5.** Raman spectra of CdS powder and CdS nanofilm grown on FTO glass substrate with the conducting side facing down

### 3.6. Growth process and reaction mechanism analysis

In this work, Fig. 6 disclosed the possible growth mechanism of the as-prepared CdS nanofilm with the conductive side of FTO glass substrate facing down and the numbers represented chemical reaction and evolutionary process. Initially,  $\text{CdCl}_2 \cdot 2.5\text{H}_2\text{O}$  was dissociated to form  $\text{Cd}^{2+}$  ion (Eqs. 1). Under the low temperature, Tu was partially hydrolyzed to form  $\text{S}^{2-}$  ion (Eqs. 2) [25]. A small amount

of CdS nuclei can be formed with  $\text{Cd}^{2+}$  and  $\text{S}^{2-}$  (Eqs. 6). However, there was a narrow interface between the conductive side of FTO glass substrate facing down and the bottom of the autoclave.

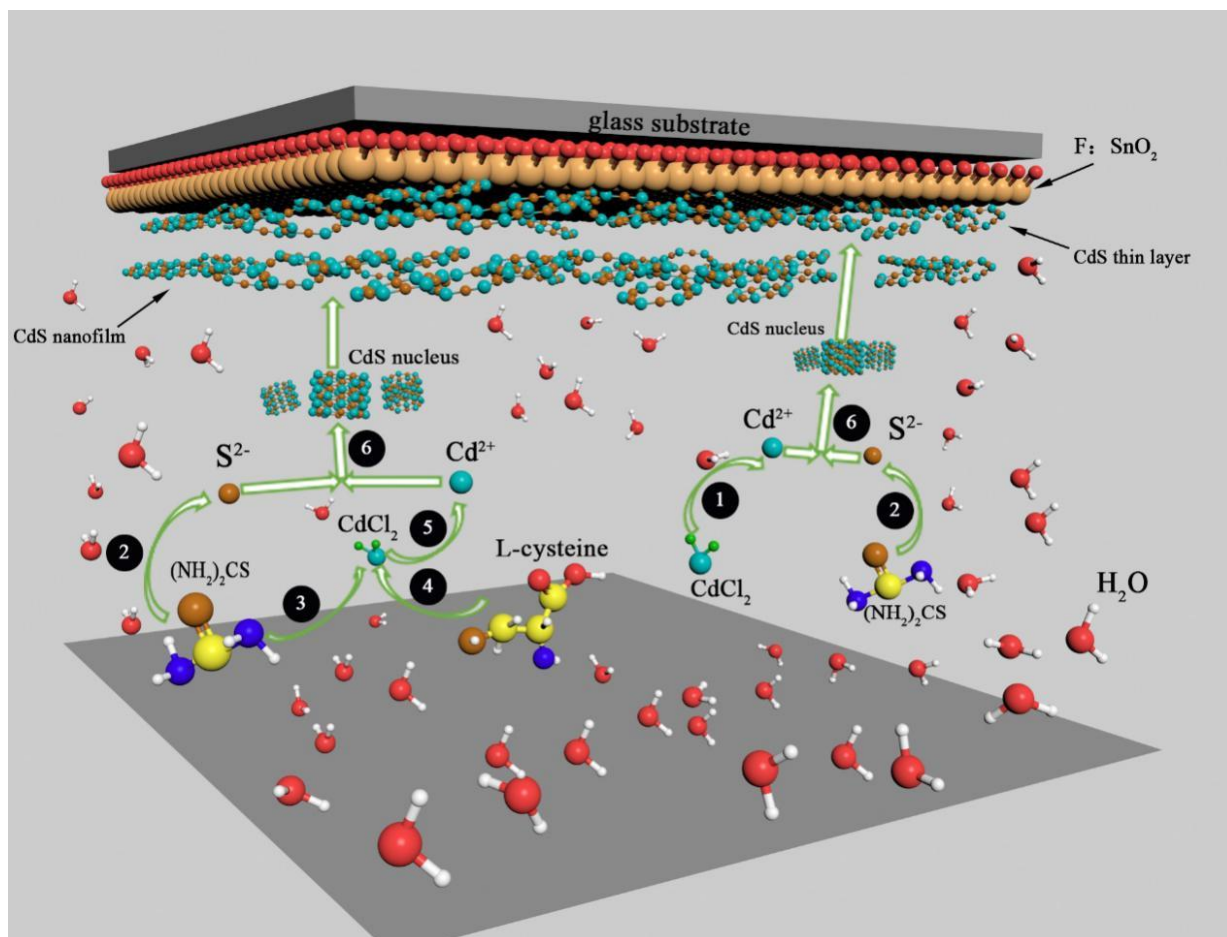
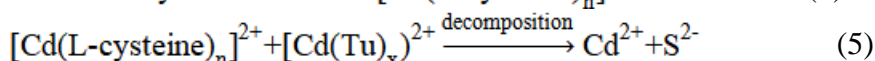
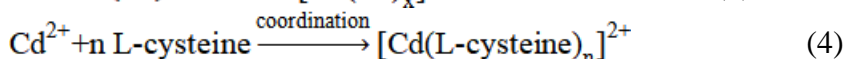
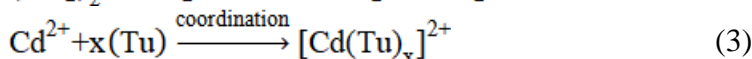
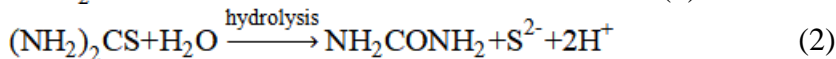
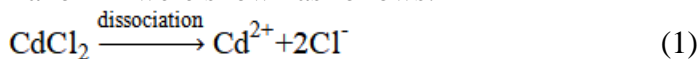


**Figure 6.** Growth mechanism of CdS nanofilm grown on FTO glass substrate with the conducting side down

In the initial reaction, the temperature difference was generated in the solution of the autoclave. The CdS nuclei might be transported onto the conductive side of the FTO glass substrate in the narrow interface due to strong convection [26]. Besides, the minimum value of the conduction band of the  $\text{SnO}_2/\text{CdS}$  interface coincided, and it was also beneficial to the ohmic contact between  $\text{SnO}_2$  and CdS [27]. Therefore, the CdS nuclei might gradually grow into CdS thin layer on the conductive side of the FTO glass substrate. Meantime, Tu as a strong ligand with  $\text{Cd}^{2+}$  can form stable  $[\text{Cd}(\text{Tu})_x]^{2+}$  complexes ((Eqs. 3), the stability constant  $\log\beta_x=3.55$ ) [28]. When the temperature was raised,  $\text{S}^{2-}$  ion concentration was significantly increasing with Tu rapidly hydrolyzed (Eqs. 2). At the same time, L-cysteine can be dissolved in deionized water and be regarded as a sulfur source to promote the  $\text{S}^{2-}$  ion concentration. Besides, there were various functional groups in the L-cysteine molecule, such as amines groups ( $-\text{NH}_2$ ), carboxyl groups ( $-\text{COOH}$ ), and mercaptan groups ( $-\text{SH}$ ). These functional groups can coordinate well with inorganic cations and metal to form  $[\text{Cd}(\text{L-cysteine})_n]^{2+}$  complexes

(Eqs. 4), and it has been confirmed based on mass spectrometry by Burford et al. [29]. When the temperature continued to rise, L-cysteine and Tu gradually escaped from two complexes, respectively, releasing a large amount of  $\text{Cd}^{2+}$  ions at a certain temperature (Eqs. 5). At this time,  $\text{Cd}^{2+}$  and  $\text{S}^{2-}$  ion combined with growing into many CdS nuclei (Eqs. 6). CdS had a large electric dipole moment [30], and the electrostatic attraction of the dipole moment generated a Van der Waals force. It might promote the transport of the CdS nuclei onto the CdS thin layer. Finally, the CdS nuclei adhered to CdS thin layer, and it grew into hexagonal CdS nanofilm. Possible chemical reaction and evolutionary process of CdS nanofilm were shown as follows:



### 3.7 Electrical performance analysis

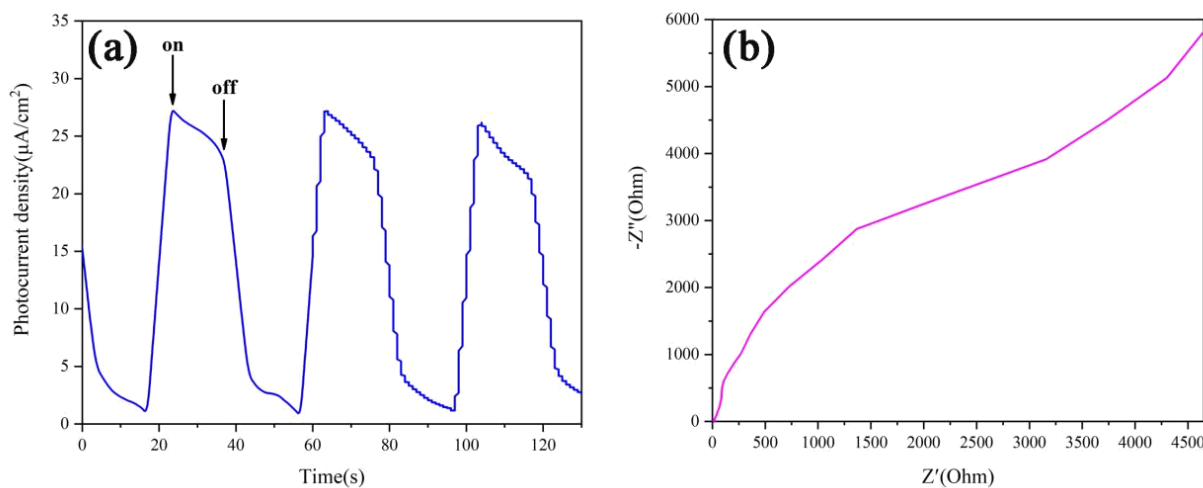


**Figure 7.** (a) Photocurrent density-time curve and (b) EIS of CdS nanofilm grown on FTO glass substrates with conducting side facing down

The transient photocurrent response and EIS of CdS nanofilm were measured under visible light irradiation, as shown in Fig. 7. The transient photocurrent response of CdS nanofilm with an area of  $1 \text{ cm}^2$  was measured in  $0.5 \text{ M Na}_2\text{SO}_4$  solution at a fixed electrode potential of  $1.23 \text{ V}$  versus RHE. It can be observed from Fig. 7 (a) that when the light was on, the photocurrent increases rapidly and decay slightly, and then kept a constant value. However, when the light was turned off, the photocurrent decreases rapidly. In the 120 s cycle test, the photocurrent has good reducibility. The reason for this phenomenon might be [31-32]: the separation of electron-hole pairs at the interface of

CdS nanofilm / electrolyte generated the initial current. At this time, the hole was trapped or occupied by the reducing substance in the electrolyte. Electrons were transported to the cathode through hexagonal CdS nanofilm and the conductive side of FTO glass substrate. However, the slight decay of photocurrent might be [33]: some of the holes were not trapped or captured by the reducing substance in the electrolyte, recombined with the electrons in the conduction band. When the hole was combined with the electron, the generation and transfer of the electron-hole pairs reached a balance, forming a relatively constant current. Therefore, the samples exhibited faster and reproducible photocurrent response upon each illumination, owing to the better crystallinity and more compact contact between CdS nanofilm and FTO glass substrate. In order to further explore migration and conversion of the electron-hole pairs, as shown in Fig.7 (b), EIS of CdS nanofilm was measured under visible light irradiation. In Fig.7 (b), the radius of the circle on the Nyquist curve related to the photoreaction rate of the sample on the electrode surface. However, Fig.7 (b) was similar to a sector with a small radius, indicating that the chemical impedance of CdS nanofilm on the electrode surface was low and the charge transfer rate was fast.

#### 4. CONCLUSIONS

In summary, hexagonal wurtzite CdS nanofilm was successfully prepared on the FTO glass substrate with the conductive side facing down via the hydrothermal method. SEM found that it was not conducive to grow CdS nanofilm on the FTO glass substrate with the conductive side facing up. On the contrary, the CdS nanofilm with the conductive side of the FTO glass substrate facing down uniformly adhered to the conductive side, showing a hexagonal shape. Meanwhile, further detailed explorations showed here to demonstrate that the as-prepared samples had a better crystallinity. The PL optical spectrum and the Raman spectrum were used to analyze the optical properties of the sample. The results indicated that both of spectra demonstrated a slight redshift. Besides, the two possible growth mechanism of CdS nanofilm on the FTO glass substrate was discussed: growth of CdS thin layer and CdS nanofilm. The transient photocurrent response and EIS were used to study the electrical properties of CdS nanofilm. The results showed that the photocurrent of CdS nanofilm had good reducibility and CdS nanofilm had the characteristics of low chemical impedance and fast charge transfer rate. Compared with the related reports, a rather facile route was proposed to prepare a uniform and dense hexagonal CdS nanofilm on the FTO glass substrate. At the same time, the CdS nanofilm grown on FTO glass substrates via hydrothermal method also provided a basis for the application of electronic transport layer of solar cell.

#### ACKNOWLEDGMENTS

This work is supported by the National Laboratory of Solid State Microstructures, Nanjing University (Grant No. M32060); Scientific Research Program of the Higher Education Institution of Xinjiang (Grant No. XJEDU2020Y038); and Natural Science Foundation Project of Xinjiang Uygur Autonomous Region (Grant No. 2019D01C001 and 2019D01C002); Xinjiang Uygur Autonomous Region Department of Education (Grant No. XJ2020G305 and XJ2020G306). We would like to acknowledge it for financial support.

## References

1. R. A. G. Shaikh, S. A. More, G. G. Bisen, S. R. Jadkar, J. V. Sali and S. S. Ghosh, *Journal of Materials Science: Materials in Electronics*, 30 (2019) 20354.
2. H. A. Mohamed, *Thin Solid Films*, 589 (2015) 72.
3. S. R. Gosavi, C. P. Nikam, A. R. Shelke, A. M. Patil, S.-W. Ryu, J. S. Bhat and N. G. Deshpande, *Materials Chemistry and Physics*, 160 (2015) 244.
4. S. Arya, A. Sharma, B. Singh, M. Riyas, P. Bandhoria, M. Aatif and V. Gupta, *Optical Materials*, 79 (2018) 115.
5. X. D. Yang, J. Ma, T. L. Wang, B. Y. Wang, D. W. Meng and Y. Q. Wang, *New Journal of Chemistry*, 43 (2019) 10126.
6. S. S. Fang, M. Y. Sun, Y. W. Zhou, Q. Liang, Z. Y. Li and S. Xu, *Journal of Alloys and Compounds*, 656 (2016) 771.
7. X. X. Jiang, F. Chen, H. Xu, L. G. Yang, W. M. Qiu, M. M. Shi, M. Wang and H. Z. Chen, *Solar Energy Materials and Solar Cells*, 94 (2010) 338.
8. K. He, M. Wang and L. J. Guo, *Chemical Engineering Journal*, 279 (2015) 747.
9. K. Kaviyarasu, E. Manikandan and M. Maaza, *Journal of Alloys and Compounds*, 648 (2015) 559.
10. F. Li, S. M. Wu, L. J. Zhang and Z. Li, *Journal of Materials Science: Materials in Electronics*, 28 (2017) 16233.
11. M. Ouafi, B. Jaber and L. Laânab, *Superlattices & Microstructures*, 129 (2019) 212.
12. D. Y. Yang, X. H. Zhu, Z. R. Wei, W. Q. Yang, L. Z. Li, J. Yang and X. Y. Gao, *Journal of Semiconductors*, 32 (2011) 15.
13. M. Thambidurai, N. Muthukumarasamy, N. Murugan, D. Velauthapillai, S. Agilan and R. Balasundaraprabhu, *Applied Physics A*, 104 (2011) 1129.
14. Y. X. Guo, J. C. Jiang, S. H. Zuo, F. W. Shi, J. H. Tao, Z. G. Hu, X. b. Hu, G. J. Hu, P. X. Yang and J. H. Chu, *Solar Energy Materials and Solar Cells*, 178 (2018) 186.
15. X. W. He, W. F. Liu, C. F. Zhu and S. J. Guo, *Chinese Journal of Chemical Physics*, 24 (2011) 471.
16. A. Abdel-Galil, M. R. Balboul, A. Atta, I. S. Yahia and A. Sharaf, *Physica B: Condensed Matter*, 447 (2014) 35.
17. D. Zhong, B. Cai, X. L. Wang, Z. Yang, Y. D. Xing, S. Miao, W. H. Zhang and C. Li, *Nano Energy*, 11 (2015) 409.
18. B. H. Zhang, F. Q. Guo, L. H. Yang and J. J. Wang, *Materials Research Innovations*, 19 (2015) 60.
19. H. N. Bai, F. Q. Guo, B. H. Zhang, L. T. Gai and R. Q. Guo, *Journal of Materials Science: Materials in Electronics*, 29 (2018) 9193.
20. B. Edward Boone and C. Shannon, *Journal of Physical Chemistry A*, 100 (1996) 9480.
21. J. H. Shen, S. W. Yeh, H. L. Huang and D. Gan, *Thin Solid Films*, 519 (2012) 549.
22. H. Zeng, G. Duan, Y. Li, S. Yang, X. Xu and W. Cai, *Advanced Functional Materials*, 20 (2010) 561.
23. L. Spanhel and M. A. Anderson, *Journal of the American Chemical Society*, 112 (1990) 2278.
24. S. H. Yu, Y. S. Wu, J. Yang, Z. H. Han, Y. Xie, Y. T. Qian and X. M. Liu, *Chemistry of materials*, 10 (1998) 309.
25. A. Phuruangrat, T. Thongtem and S. Thongtem, *Materials Letters*, 63 (2009) 1538.
26. J. S. Wu and H. M. Li, *Journal of Salt Science and Chemical Industry*, 04 (2004) 22.
27. D. W. Niles, D. Rioux and H. Höchst, *Journal of applied physics*, 73 (1993) 4586.
28. Y. D. Li, H. W. Liao, Y. Ding, Y. T. Qian, L. Yang and G. E. Zhou, *Chemistry of Materials*, 10 (1998) 2301.
29. N. Burford, M. D. Eelman, D. E. Mahony and M. Morashb, *Chemical Communications*, 1 (2003) 146.
30. H. X. Chang, X. J. Lv, H. Zhang and J. H. Li, *Applied physics Letters*, 12 (2010) 483.
31. G. P. Dai, J. G. Yu and G. Liu, *Journal of Physical Chemistry C*, 115 (2011) 7339.

32. J. G. Yu and B. Wang, *Applied Catalysis B Environmental*, 94 (2010) 295.

33. J. G. Yu, Y. Wang and W. Xiao, *Journal of Materials Chemistry A*, 36 (2013) 10727.

© 2020 The Authors. Published by ESG ([www.electrochemsci.org](http://www.electrochemsci.org)). This article is an open access article distributed under the terms and conditions of the Creative Commons Attribution license (<http://creativecommons.org/licenses/by/4.0/>).